Laser interferometric flow measurements in the lateral line organ

Tsang, P

2 Temperature dependence of the viscosity of lateral line canal fluid

Introduction

Lateral line organs such as the ones found on the head of the ruffe are used by the animal to detect water motion around it (Dijkgraaf, 1963). The supraorbital lateral line organ of the ruffe consists of bony canals with a number of neuromasts located under bony bridges. Neuromasts are the sensory elements of the lateral line organ and are constructed from dome shaped extracellular matrices (Kelly and van Netten, 1991), cupulae, which have bundles of sensory hair cells attached to their bases. The cupulae are stimulated by a combination of viscous and inertial fluid forces (van Netten, 1987), conveyed to them by the surrounding lateral line canal fluid. The lateral line canal fluid is in mechanical contact with the outside water via the flexible skin windows which cover the canal (van Netten and van Maarseveen, 1994).

Through these mechanical connections, energy from the outside water motion is utilised to drive the cupulae. The resultant motion of the hair bundles is transduced into receptor potentials by the hair cells. Part of the stimulus energy is lost through viscous damping from the lateral line canal fluid. To gain a better insight into the extent of energy dissipated, the viscosity of the lateral line canal fluid needs to be known.

Previous studies of the frequency response of the cupula in the ruffe has indirectly yielded a viscosity value of 5.1 mPa s for the lateral line canal fluid at a temperature of approximately 18 °C (van Netten and Kroese, 1987; van Netten, 1991). This was achieved by applying a hydrodynamic model to measurements of the frequency response of the cupula. The viscosity was calculated from the best fit through the results.

In the present paper, direct measurements are described and the effect of temperature on viscosity is also investigated. There are many types of viscometers which can be used for measuring fluid viscosity. The most well-known are based on oscillating-body, capillary-flow and falling-ball techniques (Kestin, 1988; Fung, 1981). One of the simplest type of viscometers is the oscillating-body viscometer. This uses a probe which is axially symmetrical and is designed to oscillate torsionally in the sample fluid. By measuring the torque and angular frequency, the viscosity can be determined.

A type of viscometer that is applicable to the measurement of viscosity in a volume of about 0.1 ml sample fluid, is the oscillating magnetic microrheometer (Lutz *et al.*, 1973). With this technique a small iron sphere is driven by a magnetic field in a small volume of sample fluid and its displacement is measured. Using a mathematical model the viscosity of the fluid can be obtained. The fact that 0.1 ml is needed makes it unsuitable for measuring lateral line canal fluid viscosity, because only ≈ 0.04 ml can be obtained from one fish.

An alternative use of an oscillating-body is employed by the technique described in this paper (see Fig. 1). Instead of measuring the angular frequency and torque of a probe performing torsional oscillations, the resonance characteristics exhibited by an oscillating sphere performing swinging oscillations in a sample fluid are utilised. The Q_{3dB} value of the resonance peak depends upon the sample fluid's viscosity. The Q_{3dB} value is given by the ratio $f_0 / (f_h - f_l)$ where f_0 is the resonance frequency, f_l and f_h are the frequencies at which the response is 3 dB lower than the maximum with $f_l < f_0 < f_h$.

Prior to the determination of the sample fluid's viscosity, a graph of experimentally measured Q-factors versus viscosity is made from a series of glycerol/water mixtures with known viscosities. The viscosity range made up by the glycerol/water mixtures is chosen to cover the expected sample fluid's viscosity. Then the measured Q-factor of the sample fluid is used to find its corresponding viscosity from the graph.

The method of measuring viscosity is based on a comparison method and therefore no specific hydrodynamic theory of forces on the probe and related frequency response is necessary. The accuracy is improved, however, by fitting a model through the measured frequency responses. In this way, the resonance frequency of the oscillating sphere measured in a fluid can be determined more precisely. This in turn makes the process of transforming Q-factors to viscosity more accurate. Therefore a hydrodynamic model of the fluid forces on the oscillating sphere is described in the theory section.

Theory

Oscillating sphere

The oscillating sphere probe employed by the viscometer used is shown in the enlarged circle of Fig. 1. It consists of a piezo element driving a wire shaft with a

bending stiffness constant *S*. Attached to the tip of the wire shaft is a small sphere. This is submerged in the fluid of which the viscosity has to be measured. Evoked oscillatory movements of the piezo element are directly coupled to the wire shaft. As the sphere, on the other end of the wire shaft, is impeded by the fluid and because the wire is elastic, its displacement is not equal to that of the driver. The difference in displacement is determined by the hydrodynamic properties of the fluid, amongst others the viscosity.

A large part of the related theory is based on the work by Stokes (1851) on the motion of pendulums in viscous fluids and on a hydrodynamic model derived by van Netten (1991) for viscously driven spheres.

Prior to describing the motion of the sphere, a few assumptions must be made. The fluid is incompressible and Newtonian. A fluid is considered to be incompressible for a periodic flow when $v \ll c$ and $\tau \gg l/c$, where v is the velocity of the fluid, c is the speed of sound in the fluid (1500 m/s), where l and τ denote the distance and time over which the fluid flow noticeably changes (Landau and Lifshitz, 1987). These conditions for an incompressible fluid are satisfied in the present case, because the velocity of the sphere at the resonance frequency is ≈ 0.02 m/s. Also, the shortest vibration period τ is 1.25 ms and the length over which the fluid flow noticeably changes is ≈ 1 cm, hence $\tau \gg l/c$.

To linearise the fluid flow equations, the radius, a, of the sphere has to be far greater than its displacement amplitude, i.e. $a \gg X_0$. For the present measurements, a = 0.5 mm and X_0 = 10 μm and thus linearisation is justified.

Consider a wire shaft with a displacement of $u(t) = U_0 e^{i\omega t}$ driving a sphere in a viscous, incompressible Newtonian fluid which is at rest at infinity. If the sphere oscillates with a frequency ω and a displacement $x(t) = X_0 e^{i\omega t}$, then the total force exerted by the wire shaft on the sphere is given by:

$$F(t)_{wire} = \big(u(t) - x(t)\big)S = M\ddot{x}(t) + F_{fluid}, \tag{1}$$

for $a \gg X_0$ and the wire shaft length $L \gg X_0$ and with F_{fluid} (Stokes, 1851; Landau and Lifshitz, 1987) given by:

$$F_{fluid} = \frac{6\pi a^2 \mu}{\delta\omega}\left(1 + \frac{2a}{9\delta}\right)\ddot{x} + 6\pi a\mu\left(1 + \frac{a}{\delta}\right)\dot{x}, \tag{2}$$

where μ is the dynamic viscosity of the fluid, δ is the boundary layer thickness, which is given by:

$$\delta = \sqrt{\frac{2\mu}{\omega\rho}}, \tag{3}$$

with ρ being the density of the sample fluid.

Solving for $x(t)$ yields an expression for the displacement amplitude, X_0 of the sphere in complex notation:

$$X_0 = \frac{P_c U_0}{P_c - \frac{1}{9}\left(\frac{2\sigma}{\rho}+1\right)\left(\frac{f}{f_t}\right)^2 + \frac{(i-1)}{\sqrt{2}}\left(\frac{f}{f_t}\right)^{3/2} + i\left(\frac{f}{f_t}\right)} \tag{4}$$

with

$$f_t = \frac{\mu}{2\pi\rho a^2}, \tag{5}$$

$$P_c = \frac{Sa\rho}{6\pi\mu^2}, \tag{6}$$

and σ is the density of the sphere. The parameter f_t is equal to the transition frequency at which the inertial fluid force component starts to dominate over the viscous component for a periodic flow. The Reynolds number Re_{AC} for a periodic flow is equal to (f/f_t). P_c is a dimensionless parameter which plays a major role in governing the shape of frequency response along with σ/ρ, whereas U_o and f_t serve as scaling factors.

According to Eq. 4, resonance occurs when $P_c \gg 1$. A rough estimation of P_c for the sense probe used can be made using Eq. 6. The sense probe has a stiffness, S, of ≈ 40 N/m, σ = 7000 kg/m^3, a radius a = 0.5 mm and μ is expected to be between 1 to 10 mPa s. This means that P_c ranges from 10^4 to 10^6. As $P_c \gg 1$ it means that an approximation of the resonance frequency f_0 can be obtained by setting the two most significant real terms of the denominator of Eq. 4 to zero:

$$f_0 = f_t\sqrt{9P_c/(1+2\sigma/\rho)}. \tag{7}$$

Furthermore, it also means that the shape of the frequency response around the resonance frequency is determined by the first two terms of the denominator of Eq. 4. The Q-factor may be approximated by:

$$Q = \frac{\sqrt{MS}}{R}, \tag{8}$$

where M is the mass of the sphere, S is the stiffness of the wire and R is the dissipative fluid force per unit velocity. Although R is frequency dependent, the Q-factor is determined by the damping around the resonance frequency. As the resonance frequency is ≈ 500 Hz and P_c » 1, $R \approx 6\pi a^2 \mu / \delta$ (see Eq. 2), because the factor $a/\delta \approx 20 \geq 1$. Substituting M and R into Eq. 8 gives Q as a function of μ at $f = f_0$ and for P_c » 1:

$$Q = \frac{\sqrt{\frac{4}{3}\pi a^3 \sigma S}}{3\pi a^2 \sqrt{2\rho\mu\omega_0}}. \tag{9}$$

Methods

Laser Doppler interferometer

The displacement of objects moving in the submicron region can be accurately measured using laser interferometry (see Lading, 1971, or Drain, 1980). The setup shown in Fig. 1 is based on the laser interferometer as described by van Netten (1988).

Polarised light emitted from the He-Ne laser (Spectra Physics Stabilite 124B) is first rotated by a λ/2 retardation plate to ensure that the laser light is of the correct polarisation for maximum transmission through subsequent polarised beamsplitters. The beam then passes through a pair of lenses L1 and L2, which form a telescope used for correcting the Gaussian beam/lens interactions (Hanson, 1973). Following the telescope, the beam is then split by the beamsplitter BS1 and the two resulting beams then pass through a pair of Bragg-cells (Isomet 1205c-2); one of which is driven by a R.F. source of 80 MHz and the other by 79.6 MHz. Thus, there is an optical frequency difference of 400 kHz between the two emerging beams. These are subsequently directed into the prisms P_1 and P_2 via two mirrors.

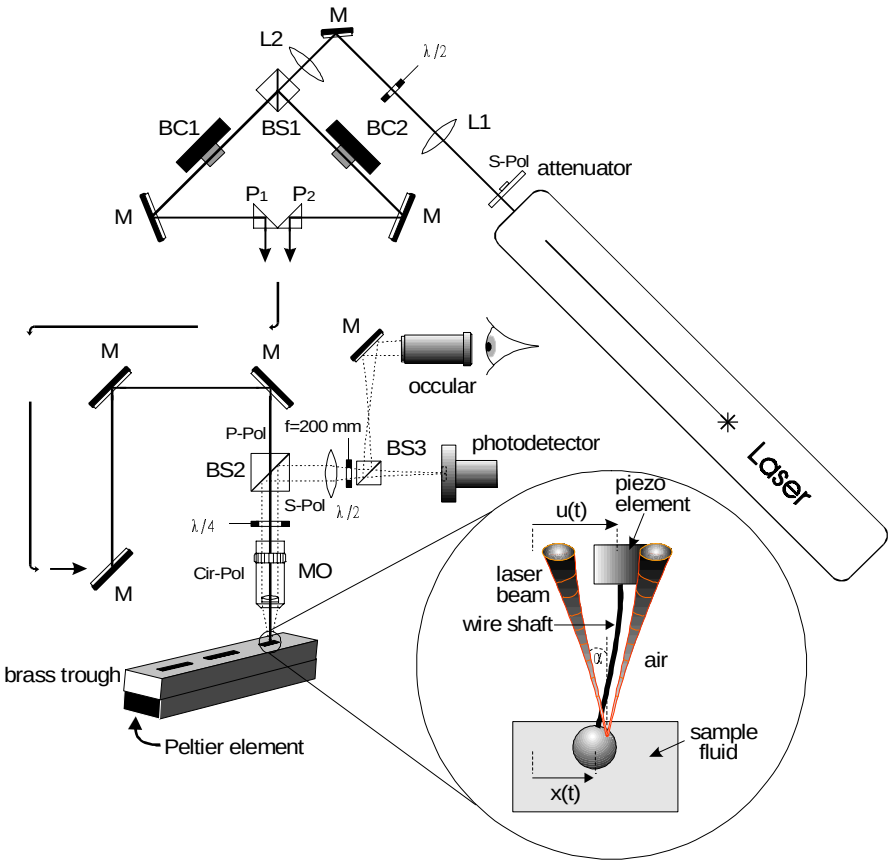

Figure 1: Diagram of the laser interferometer viscometer setup. L1 (*f*=80 mm) and L2 (*f*=200 mm) are lenses, BS1 BS2 BS3 are beamsplitters, BC1 (80 MHz) and BC2 (79.6MHz) are Bragg-cells, M are mirrors, λ/4 and λ/2 are retardation plates, P_1 and P_2 are prisms, Cir-Pol, P-Pol and S-Pol indicates polarisation, *MO* is a microscope objective lens.

After being reflected by a series of mirrors and beamsplitter BS2, the two beams are focused onto the surface of the oscillating sphere by a microscope objective lens (Zeiss Apochromat 40 mm), thus forming a fringe pattern. The sphere's surface scatters the laser light in all directions as it moves through the fringe pattern. Some of the Doppler shifted light is scattered back in the direction of the objective lens and is collected. It is then focused onto a photodiode via BS2.

The laser light intensity is conserved as much as possible by the effective use of polarisation. Light falling on the beamsplitter BS2 is P-polarised and passes directly through. P-polarised light is then converted to circularly polarised light by the λ/4 retardation plate as it travels towards the microscope objective lens. Backscattered circularly polarised light returning via the optical axis is converted to S-polarised light by the same λ/4 plate and is now reflected by BS2. This S-polarised light can then be redirected via BS3 towards the ocular or to the photodiode by adjusting the λ/2 plate located in front of BS3.

The sensitivity of the interferometer can be adjusted by varying the distance between the two beams, simply by moving the two prisms P_1 and P_2 in tandem, backwards or forwards. This has the effect of increasing or decreasing the fringe spacing of the fringe pattern as the angle (α) between the beams and the optical axis at the focus point is varied. The fringe spacing $\lambda_{fringe} = \frac{\lambda}{2n\sin\alpha} = \frac{v}{\Delta f}$ is governed by the angle α, where n is the refractive index and λ the laser wavelength. The velocity of the moving sphere v is then given by the modulation frequency Δf multiplied by the fringe spacing.

The photodiode signal is amplified and frequency demodulated by a demodulator (Polytec VIB-VDEC) to give a voltage which is proportional to the velocity of the sphere. The signal from the demodulator is sampled and averaged by a spectrum analyser (2034, Brüel & Kjær).

Oscillating sphere

A steel sphere (∅ 1 mm) taken from a Parker ball-point cartridge (Parker™, fine point) is used as the sense probe. A hole of 0.3 mm in diameter was drilled through the steel sphere and a short length of tungsten wire (9.3 mm in length, ∅ 0.3 mm) was glued in with epoxy resin. This unit was then attached to a piezo element (Physik Instrumente) which was driven by a pseudo-random noise signal of 3-800 Hz generated by the spectrum analyser.

Calibration fluids

In the present measurement technique, the Q-factor of a measured resonance curve of a sample fluid is compared to that of a series of calibration fluids with known viscosities. This means that the calibration fluids must have a similar density with respect to the sample fluid for the resonance frequency to be in the same region (see Eqs. 7 and 9).

The density of the supraorbital lateral line canal fluid is very close to that of water (1010 kg/m^3, Jielof *et al.*, 1952) and this led to the choice of using different glycerol/water mixtures. Glycerol-water mixtures have densities close to that of the lateral line canal fluid and, furthermore, viscosity data on glycerol/water mixtures are readily available.

Glycerol/water weight data were taken from the Handbook of Chemistry and Physics (1979) and converted and plotted as a series of points to give a graph of viscosity versus glycerol/water volume ratio (see Fig. 2) ($\rho_{glycerol}$ =1260 kg/m^3).

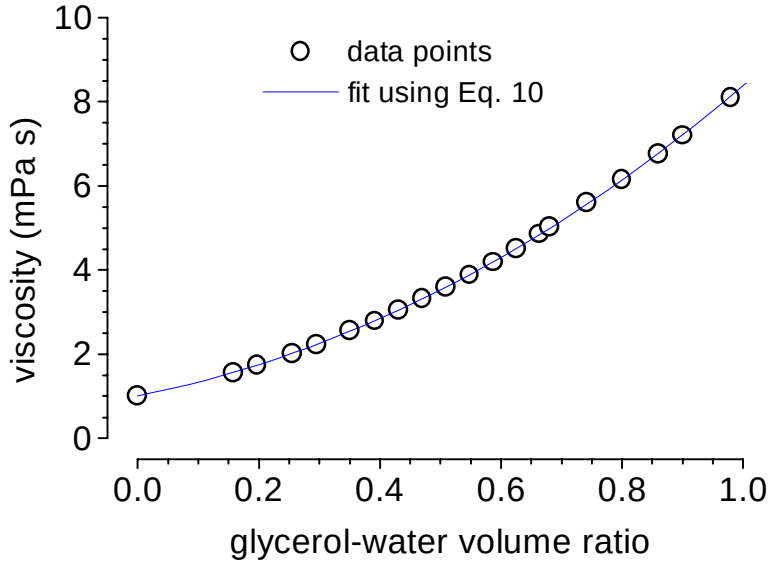

Figure 2: Viscosity as a function of glycerol/water volume ratio at 20 °C. The solid line is a fit made with Eq. 10 through the data taken from the Handbook of Chemistry and Physics (1979).

By use of a curve fitting routine an empirical relationship between viscosity and glycerol/water volume ratio was obtained as:

$$\mu = -28.2x + 118.3e^{0.263x} - 117.3, \quad (10)$$

where μ is the viscosity in mPa s and x is the glycerol-water volume ratio.

Using the graph as depicted in Fig. 2, a series of calibration fluids was produced, starting with a viscosity of 1 mPa s and ending with the final mixture of 10 mPa s with increments of 1 mPa s per mixture. This viscosity range was used for pilot experiments to roughly determine the range that covered the sample fluid's viscosity. After this, a viscosity range with finer steps was used for increased accuracy. For these experiments a viscosity range from 1 to 3 mPa s with increments of 0.25 mPa s was used. For every mix required, the precise volume ratio needed was calculated and with the use of a 1 ml hypodermic syringe precise volumes of glycerol and water were mixed.

A series of frequency response measurements on glycerol/water mixtures were carried out at 20 °C, because the standard data in the literature are quoted for 20 °C. The resultant resonance curves were then curve fitted to obtain the Q-factor for each solution (see Figs. 3 and 4). This was used for the comparison with the Q-factors of resonance curves belonging to the lateral line canal fluid measured at temperatures ranging from 4 to 20 °C. This particular temperature range was chosen, because it is close to the temperatures of the ruffe's habitat.

For each new temperature setting, a period of approximately 2 minutes was allowed to elapse before new recordings were made. This gave the sample fluid time to adjust and stabilise to the new temperature setting of the Peltier cooled brass trough.

Preparation

The fishes, *Acerina cernua* L. used in these experiments were anaesthetised by I.P. injection with Saffan (Pitman-Moore) (Oswald, 1978). For the present experiments 8 fishes were used.

Approximately 15 minutes after applying the anaesthetic, the lateral line canal fluid was extracted from the supraorbital canal using a 1 ml hypodermic syringe. A fish has on average approximately 0.04 ml of lateral line fluid in the supraorbital canal.

Prior to the extraction of the lateral line canal fluid, the fish were always taken out of the water tank to avoid mixing the lateral line canal fluid with water external to the fish.

The contents of the syringe was then carefully emptied into a Peltier cooled brass trough. The oscillating sphere was then lowered into the fluid until it was submerged by 0.1 mm similar to the procedure used for the measurement of the calibration fluid viscosity. All the air bubbles were removed and the depth of the fluid in relation to the oscillating sphere was kept as constant as possible by close inspection throughout the duration of the experiment.

Results

Typical examples of frequency responses of the oscillating sphere measured in some of the glycerol/water fluids and the lateral line canal fluid are shown in Fig. 3. At 20 °C, the fluid with the lowest viscosity (1 mPa s) has the highest peak and the fluid with the highest viscosity (3 mPa s) has the lowest peak. It is clear to see that the peaks do not share the same resonance frequency, f_0. There is a frequency shift of 4 Hz from approximately 467 Hz for μ = 1 mPa s to 463 Hz for μ = 3 mPa s.

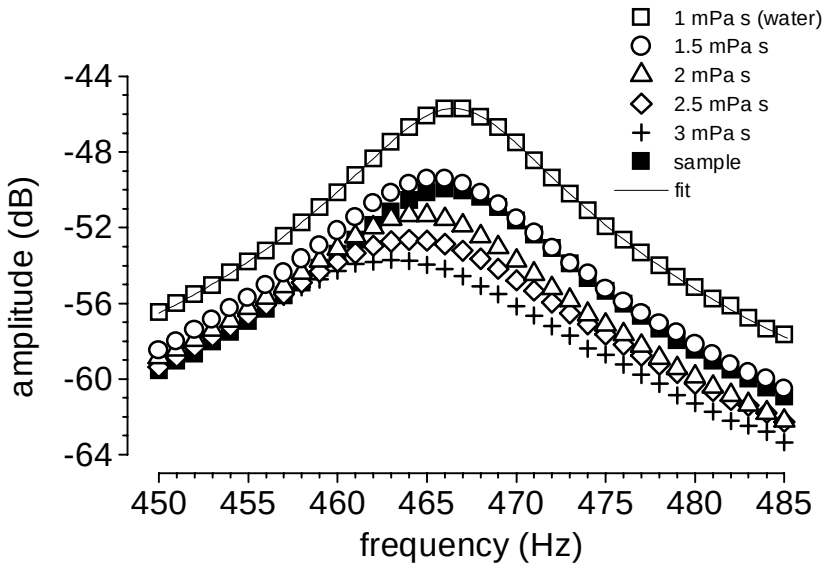

Figure 3: Frequency responses of the oscillating sphere measured at a depth of 0.1 mm for a range of calibration fluids and a sample fluid. All the frequency responses were measured at 20 °C. The solid line shows a fit of the water measurements with a second order filter model.

The resonance peak for lateral line canal fluid has a resonance frequency f_0 = 466 Hz, which is very slightly lower than that of water (μ = 1 mPa s).

The Q-factors of frequency responses measured in a complete set of glycerol/water mixtures are plotted in Fig. 4 as a function of viscosity (μ). The Q-factor of the lateral line fluid converted to a measure of viscosity is indicated by the dotted lines.

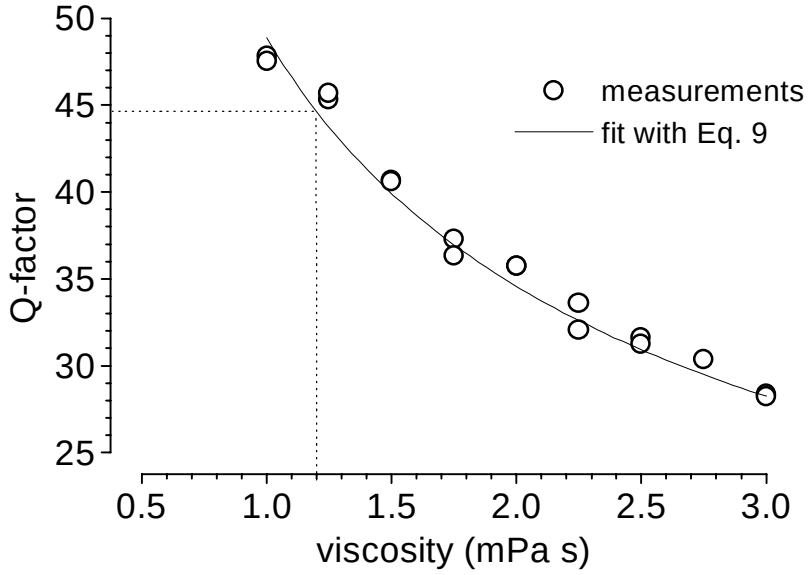

Figure 4: Q-factor against viscosity for the different calibration mixtures. The continuous line is a fit through the measurement points using equation 9. The values for the fit are σ = 7000 kg/m^3, S = 32 N/m, a = 5×10^{-4}, f_0 = 467 Hz and ρ = 1010 kg/m^3. The point of intersection of the dotted lines indicates the Q-factor measured in the lateral line canal fluid at 20 °C and the corresponding viscosity.

Fitting the data points with equation 9 yields a function which is used for converting the Q-factor of the frequency response measured in the lateral line canal fluid to the corresponding viscosity at various temperatures. These actual parameters from the fit closely match the parameters based on the physical dimensions of the oscillating sphere.

Out of the total of 8 specimens used, results taken from 4 fishes are plotted in Fig. 5 as a function temperature. Included in this figure are data points for water

taken from the Handbook of Chemistry and Physics (1979) and from actual measurements on water using the viscometer.

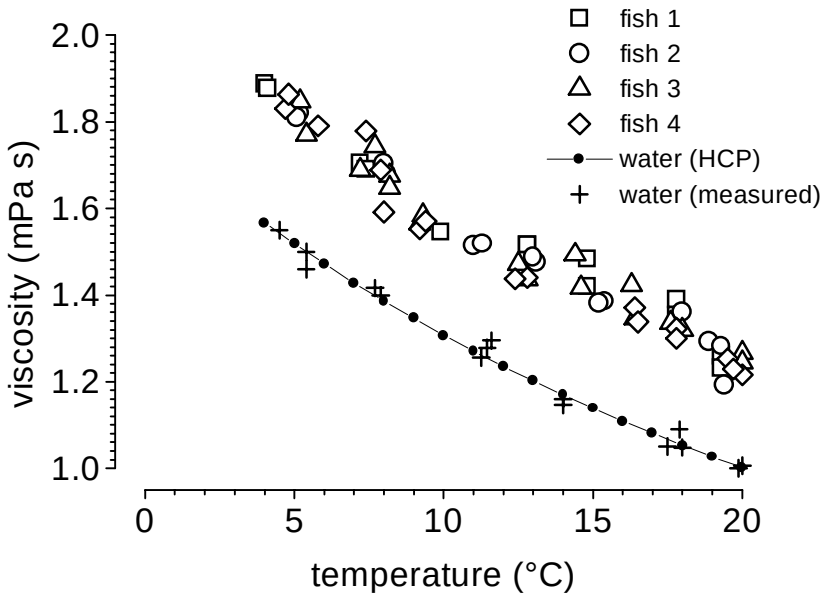

Figure 5: Results for 4 different fishes and for water are plotted as a function of temperature. The continuous curve with small black dots represents the viscosity of water as taken from the Handbook of Chemistry and Physics (1979).

It is clear that temperature has a significant effect on the viscosity of the lateral line canal fluid. At a temperature of 4 °C, the viscosity is approximately 1.90 mPa s, and it is therefore approximately 0.30 mPa s higher than that of water. At 20 °C the lateral line canal fluid viscosity decreases to a value of around 1.26 mPa s and this is 0.26 mPa s higher than that of water. This upward shift of approximately 0.30 mPa s in viscosity as compared to that of water holds for the entire temperature range for which the measurements were conducted.

The reliability of the measurement technique can be gained by the measurements with water from 5 to 20 °C. A comparison of these results to standard water viscosity data gives a precise indication of the accuracy of the glycerol/water mixtures and the overall performance of the technique.

The error in the measurement of the temperature is 0.25 °C due to the Peltier element reacting to the feedback signals sent back by the temperature sensor

embedded into the brass trough. The maximum error that can occur in the determination of the viscosity is predominantly dependent on the error that can occur in the measurement of the Q-factor. The maximum error in the measurement of the Q-factor due to the fluid level not being held constant is approximately 5%. This translates to an error of 0.08 mPa s at μ = 1.20 mPa s and 0.20 mPa s for μ = 1.90 mPa s. The error increases with viscosity because at high viscosity a relatively smaller span in the Q-factor covers a larger viscosity range.

Discussion

The relative simplicity of the measurement technique presented makes it possible to measure viscosity of small sample volumes both quickly and reliably. Temperature effects can also be easily investigated by using a built-in Peltier element.

It is clear from Fig. 3 that there is a systematic shift downwards in the resonance frequency with increasing viscosity for the different glycerol/water mixtures. This reflects the dependence of f_0 on ρ which changes with the mixtures, see Eq. 7. The difference in resonance frequency between the 1 mPa s solution to that of the 3 mPa s solution is less than 1% (4 Hz) of f_0. This 1% shift in f_0 only alters the Q-factor by 0.4%, whereas the difference in the densities of the glycerol/water mixtures used contribute to less than 2% difference in Q-factor. The viscosity is by far the most dominant parameter in determining the Q-factor, therefore no corrections were needed.

It is obvious from the results that the measured viscosity is much lower than the previous value of 5.10 mPa s obtained by van Netten and Kroese (1987) for a temperature of approximately 18 °C. For the natural temperature range of the ruffe (4-20 °C) the highest viscosity measured was 1.90 mPa s (4 °C) and 1.20 mPa s for the lowest (20 °C). Therefore, the difference between the results must be due to an additional factor other than temperature. The difference may be due to van Netten's model not incorporating the canal walls. This leads to an effectively higher viscosity value when fitted through the data of the cupular frequency response (e.g. van Hengel, 1996). A viscosity of 1.2 mPa s gives the best fit to measured data of cupular motion (van Netten and Kroese, 1987) when the effects of the canal walls are incorporated into the model. This explanation is further supported by the fact that the flow profile in the lateral line canal is frequency dependent and that it is severely influenced by the boundary layer of both the bony bridge and canal (Tsang and van Netten, 1997). Therefore, hydrodynamic models of the lateral line organ

should not neglect the influence of the integral structure of the bony bridge and canal walls when they are utilised for determining the viscosity.

Table I. *Viscosity of labyrinthine fluids*

Author(s)	Animal	Fluid type (Endolymph/ Perilymph)	Viscosity (mPa s)	Tempera-ture °C	Time elapsed (hours)
ten Kate & Kuiper (1970)	Pike	E	1.20 ± 0.08	23	Directly
		E	1.30 ± 0.08	22.6	60
ten Doesschate (1914)	Cod	E	1.297	0	-
	Cod (dead)	E	1.364	0	-
	Haddock	E	1.220	0	-
	Plaice	E	1.195	0	-
Rauch (1959)	Human	E	1.03-1.05	27	-
		P	1.02-1.03	27	-
Schnieder & Schindler (1964)	Guinea Pig	P	0.84-0.87	20	Directly
		P	1.15	20	2
		P	1.45	20	2-24
		E	1.00		Directly
Steer (1967)	Human	E	0.852 ±2%	35	Directly and
	Human	P	0.802 ±2%	35	after 1-7 days
	Cat	P	0.78 ±2%	35	

The temperature dependence of lateral line canal fluid viscosity is similar to that of water. The viscosity is, however, approximately 0.3 mPa s greater than the value of water for the temperature range of 4-20 °C. Such a dependence on temperature was also predicted by previous work on the viscosity of pike endolymph (ten Kate & Kuiper, 1970). Ten Kate & Kuiper only measured at one temperature (23 °C) but concluded that the viscosity as a function of temperature can be described by:

$$\mu = (2.31 \pm 0.16)/(1 + 0.036T + 1.85 \times 10^{-4} T^2) \qquad (11)$$

where μ is the viscosity and T is the temperature in °C. This function is based on the equation for water viscosity as a function of temperature (Tietjens, 1960). Equation 11 was then used to compare the pike endolymph viscosity to other endolymph viscosity data of other species measured at different temperature settings. Due to the lack of endolymph viscosity data measured in a single species over a range of temperature, data from other species had to be used.

Fig. 6 is an overview of the endolymph viscosity data from Table I for different species, lateral line canal fluid of the ruffe and water. Included in this graph is a plot of the viscosity function for water (Tietjens, 1960), a fit of the pike endolymph data with Eq.11 and a fit of the lateral line canal fluid data with Eq. 11 with the nominator as a free parameter.

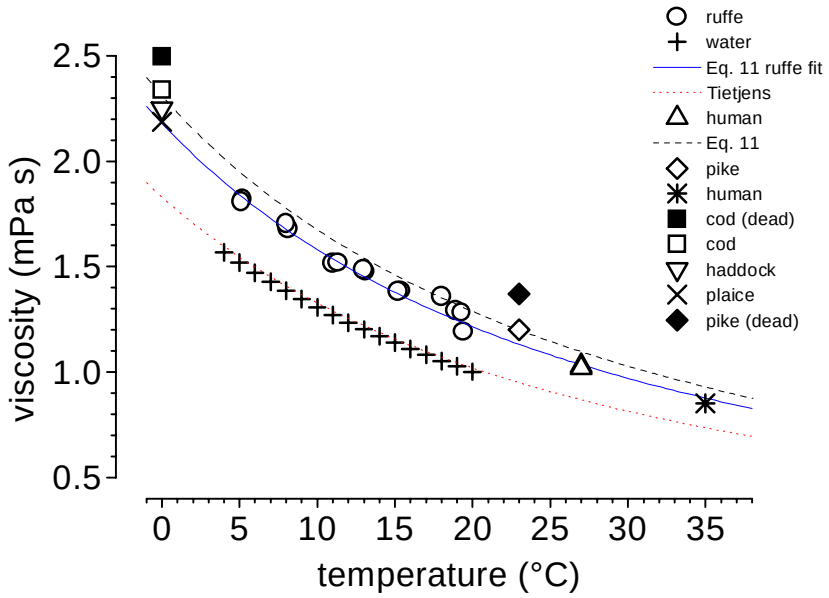

Figure 6: A plot of the endolymph viscosity data from Table I for different species, lateral line canal fluid of the ruffe and water. Two human endolymph data points are indicated by the star symbol (Steer, 1967) and the triangle symbol (Rauch, 1959). Included in this graph is a plot of the viscosity function for water (Tietjens, 1960), a fit of the pike endolymph data with Eq. 11 and a fit of the ruffe lateral line canal fluid data with $\mu = 2.18/(1+0.036\,T+1.85\times10^{-4}\,T^2)$.

Fitting Eq. 11 through the viscosity data measured in the ruffe yields a nominator of 2.18 instead of 2.31 used for the pike endolymph. This is within the error margin of the nominator of equation 11. This fit to the lateral line data passes closely through most of the data points for human, pike, plaice, cod and haddock endolymph. Only the data measured in dead animals do not fit closely. This suggests that the endolymph belonging to different species all have similar viscosity characteristics in relation to temperature. Naturally, different species function at different temperatures and hence the viscosity of the endolymph is dependent upon this.

The relationship between viscosity and temperature is often neglected in the field of macro mechanical cochlea modelling. Frequently endolymph and perilymph are assumed to have the viscosity of water (1 mPa s). A prediction of what the endolymph in mammals could be, can be obtained by extrapolating the fit through the lateral line canal fluid to 37 °C. The viscosity of endolymph at a temperature of 37 °C is expected to be $\mu = 0.84$ mPa s. The fit also gives a viscosity of 0.87 mPa s at 35 °C, which differs by less than 3% from the measured human endolymph viscosity.

There is clear evidence that time (postmortem) has an effect on the viscosity. Measurements in fluids taken from animals which have been dead for some time show a noticeable increase in viscosity. This increase can be as much as ≈ 30 % over a period of 2 hours, as can be seen from guinea pig measurements (Schnieder & Schindler, 1964). A further increase to 66 % was observed in the period between 2-24 hours. Furthermore, ten Kate & Kuiper (1970) observed an increase from 1.2 to 1.3 mPa s for the pike endolymph after the pike's head has been in the refrigerator for 60 hours and ten Doesschate (1914) also reported an increase for cod endolymph from 1.279 to 1.364 mPa s (time after death is not known). Only Steer (1967) reported that no observable change occurred in the viscosity of human endolymph after a day and for up to a week. Increase in viscosity was not observed in the measurements of the lateral line canal fluid because the experiments took less than 45 minutes to complete. This agrees with ten Kate's & Kuiper's (1970) observation that experiments conducted within 60 minutes after death showed no noticeable change in viscosity.

One other point of concern is the effect on the lateral line fluid by lowering the temperature and then increasing it. The first measurements were made at 20 °C and thereafter the temperature was lowered to 4°C. Further measurements were then made with the temperature being increased in small steps until 20°C was reached. Over a duration of around 45 minutes, no significant differences was seen between the first measurement at 20 °C and the last measurement at the same temperature. Therefore, varying the temperature does not seem to produce irreversible effects on the viscosity.

Conclusion

The method employed by our viscometer for measuring the viscosity of a fluid with a volume of 0.04 ml or less has proved to be simple and yet able to deliver reproducible results. The system can be refined further to enhance its sensitivity and accuracy by using smaller spheres and wire shafts with different bending

stiffness constants. An additional advantage of this measurement technique is that it can also be used for *in vivo* measurements. *In vivo* measurements were not conducted in the ruffe due to the difficulties of avoiding the contamination of the lateral line fluid with the water around the fish. Moreover, the temperature could not be varied with ease.

We can further conclude that the viscosity of the lateral line canal fluid is temperature dependent and ranges from 1.2 ± 0.1 mPa s at 20 °C to 1.9 ± 0.2 mPa s at 4 °C (physiological temperature range of the ruffe). The lateral line canal fluid thus has viscosity characteristics (as a function of temperature) which are very similar to those of endolymph from other species.

Throughout the duration (45 minutes) of the experiments, there were no detectable changes in the viscosity of the lateral fluid due to deterioration caused by time or by varying the temperature from 20 °C to 4°C and then back again. Although the viscosity did not change over the 45 minutes of measurement time, the viscosity is, however, expected to increase if the measurement period would be longer than 45 minutes.

Finally, the results of this study imply that hydrodynamic models of the lateral line organ must include the effects of the canal walls and bony bridge.

Acknowledgements

We would like to thank J. Land, E. Zevenberg and J. van Maarseveen for their help with the building of our apparatus and electronics. In addition we are grateful to Prof. Dr. H. Duifhuis for his helpful discussions and comments on improving this manuscript.

The investigations were supported by the Life Sciences Foundation (SLW), which is subsidized by the Netherlands Organization for Scientific Research (NWO).

References

Dijkgraaf, S. (1963). The functioning and significance of the lateral line organs. *Biol. Rev.* **38**, 51-105.

Doesschate, G. ten (1914). Onderzoekingen gedaan in het Fysiologisch Laboratorium der Utrechtse Hogeschool 5e reeks XIV. De eigenschappen van de endolymph in Beenvisschen.

Drain L. E. (1980). The laser Doppler technique. Wiley, New York.
Fung, Y. C. (1981). Biomechanics mechanical properties of living tissues. Springer-Verlag, New York.
Handbook of chemistry and physics, 60th edition. (1979). R. C. Weast and M. J. Astle (eds.). The Chemical Rubber Company.
Hanson, S. (1973). Broadening of the measured frequency spectrum in a differential laser anemometer due to interference plane gradients. *J. Phys. D: Appl. Phys.* **6**, pp. 164-171.
Hengel, P. J. W. van (1996). Emissions from cochlear modelling. Thesis, University of Groningen.
Jielof, R., Spoor, A., and de Vries, H. (1952). The microphonic activity of the lateral line, J. Physiol. **116**, pp. 137-157.
Kate, J. H. ten and Kuiper, J. W. (1970). The viscosity of the pike's endolymph. *J. Exp. Biol.* **53**, pp. 495-500.
Kelly, J. P., and Netten, S. M. van (1991). Topography and mechanics of the cupula in the fish lateral line. I. Variation of cupular structure and composition in three dimensions. *J. Morphol.* **207**, 23-36.
Kestin, J., W. A.Wakeham, (1988). Transport properties of fluids. Cindas data series on material properties volume I-1
Lading, L (1971). Differential heterodyning technique. Appl. Opt. **10** pp. 1943-9
Landau, L. D., Lifshitz, E. M. (1987). *Fluid Mechanics* (Pergamon, Oxford), 2nd ed.
Lutz, R. J., Litt, M., and Chakrin, L. W. (1973). *Rheology of biological systems*, Gabelnick, H. L., and Litt, M. (eds.). Charles C Thomas, Springfield, Ill., pp. 119-157.
Netten, S. M. van (1988). Laser interferometer microscope for the measurement of nanometer vibrational displacements of a light-scattering microscope object. *J. Acoust. Soc. Am* **83**, pp 1667-1674.
Netten, S. M. van (1991). Hydrodynamics of the excitation of the cupula in the fish canal lateral line. *J. Acoust. Soc. Am.* **89**, pp. 310-319.
Netten, S. M. van and Kroese, A. B. A. (1987). Laser interferometric measurements on the dynamic behaviour of the cupula in the fish lateral line. *Hearing Res.* **29**, 55-61.
Netten, S. M. van and Maarseveen, J. Th. P. W. van (1994). Mechanophysiological properties of the supraorbital lateral line canal in ruffe (*Acerina cernua* L.). *Proc. R. Soc. Lond. B* **256,** 239-246.
Oswald, R. L. (1978). Injection anaesthesia for experimental studies in fish. *Comp. Biochem. Physiol.* 60c, pp. 19-26.
Rauch, S. (1959). La biochimie de l'endolymphe et de la périlymphe. *C. R. Soc. Franç. oto-rhino-laryng.* **56**, 238.

Schnieder, E. A. and Schindler, K. (1964). In *Biochemie des Hörorgans.* S. Rauch.

Steer, R. W. (1967). Physical properties of labyrinthine fluids and quantification of the phenomenon of caloric stimulation. *NASA SP*-**152**, pp 409-420.

Stokes, G. G (1851). On the effect of the internal friction of fluids on the motion of pendulums. *Trans. Camb. Phil. Soc*. **9**, pp. 6-106.

Tietjens, O. (1960). *Strömungslehre BD* I. Springer Verlag.

Tsang, P. T. S. K. and Netten, S. M. van (1997). Fluid flow profiles measured in the supraorbital lateral line canal of the ruff. *Diversity in Auditory Mechanics.* World Scientific, Singapore.